Wave Generation of Gravity-Driven Sediment Flows on a Predominantly Sandy Seabed

Flores, Raúl P.; Rijnsburger, Sabine; Meirelles, Saulo; Horner-Devine, Alexander R.; Souza, Alejandro J.; Pietrzak, Julie D.; Henriquez, Martijn; Reniers, Ad

DOI
10.1029/2018GL077936

Publication date
2018

Document Version
Final published version

Published in
Geophysical Research Letters

Geophysical Research Letters

RESEARCH LETTER
10.1029/2018GL077936

Wave Generation of Gravity-Driven Sediment Flows on a Predominantly Sandy Seabed

Raúl P. Flores[1,2], Sabine Rijnsburger[3], Saulo Meirelles[3], Alexander R. Horner-Devine[1], Alejandro J. Souza[4], Julie D. Pietrzak[3], Martijn Henriquez[3], and Ad Reniers[3]

[1]Civil and Environmental Engineering, University of Washington, Seattle, WA, USA, [2]Departamento de Obras Civiles, Universidad Técnica Federico Santa María, Valparaíso, Chile, [3]Department of Hydraulic Engineering, Delft University of Technology, Delft, Netherlands, [4]CINVESTAV, Mérida, Mexico

Abstract Wave-supported gravity flows (WSGFs) generate rates of sediment flux far exceeding other cross-shelf transport processes, contributing disproportionately to shelf morphology and net cross-shelf fluxes of sediment in many regions worldwide. However, the conditions deemed necessary for the formation of WSGF limit them to a narrow set of shelf conditions; they have been observed exclusively in regions where the seabed consists of very fine-grained sediment and typically co-occur with nearby river flood events. Here we document the occurrence of a WSGF event on a predominantly sandy seabed and in the absence of a preceding river flood. Our measurements confirm that the dynamics are governed by the friction-buoyancy balance observed in other WSGF and that WSGF can form in mixed grain-size environments and transport high concentrations of sand. The occurrence of WSGF on a predominantly sandy seabed suggests that they may occur under a much wider range of conditions and, given the global prevalence of sandy shelves, they may be a more frequent and more ubiquitous feature of shelf dynamics than previously thought.

Plain Language Summary The processes that exchange sediments in gently sloping ocean regions are still not well understood. Previous studies have identified wave-supported gravity flows (WSGFs) as a leading process for the exchange of muds in many regions worldwide. These sediment flows occur when wave action resuspends seabed sediment and generates a thin near-bed layer with very high concentrations that is able to move downslope due to gravity. The measurements we present here suggest that these type of flows can also move large amounts of sediments in predominantly sandy environments and therefore may occur more frequently than previously thought.

Key Points:
- Wave-supported gravity flows can contribute to cross-shelf transport and morphological evolution on sandy inner shelves
- Particle size plays a key role in determining the dynamics of the wave-supported gravity flow
- Wave-supported gravity flows may occur more frequently and in a much wider range of shelf locations than previously thought

Supporting Information:
- Supporting Information S1

Correspondence to:
R. P. Flores,
raul.flores@usm.cl

Citation:
Flores, R. P., Rijnsburger, S., Meirelles, S., Horner-Devine, A. R., Souza, A. J., Pietrzak, J. D., et al. (2018). Wave generation of gravity-driven sediment flows on a predominantly sandy seabed. *Geophysical Research Letters*, *45*, 7634–7645. https://doi.org/10.1029/2018GL077936

Received 14 MAR 2018
Accepted 15 JUN 2018
Accepted article online 6 JUL 2018
Published online 1 AUG 2018

1. Introduction

Sediment gravity flows move large amounts of sediments from deposition zones in shallow coastal areas to deeper ocean regions, contributing substantially to the morphological evolution of continental shelves (Parsons et al., 2007; Walsh et al., 2004; Wright et al., 2001; Wright & Friedrichs, 2006) and the export of sediment, with associated nutrients, contaminants and carbon, to the abyssal ocean (Puig et al., 2004, 2003). Over the last two decades, several field and modeling studies have demonstrated the importance of wave-supported gravity flows (WSGFs) to the cross-shelf transport of muds on continental shelves and have provided a description of the governing mechanisms (Macquaker et al., 2010; Ogston et al., 2000; Parsons et al.,2007; Scully et al., 2002, 2003; Traykovski et al., 2000; Wright & Friedrichs, 2006). In WSGF, turbulence and shear stress derived from wave energy resuspends bed sediment and generates a thin near-bed high concentration layer that moves downslope due to gravity. Cross-shelf gradients in near-bottom wave energy result in large amounts of deposition in regions where waves can no longer maintain sediment in suspension (Scully et al., 2002; Traykovski et al., 2007; Wright et al., 2001).

The dynamics of WSGF are thought to be governed by a force balance between the downslope gravitational component resulting from the sediment-induced buoyancy anomaly, and friction arising from flow over the stationary seabed (Scully et al., 2002; Wright & Friedrichs, 2006; Wright et al., 2001).

In its simplest form, this force balance has been written as a linearized Chezy equation (Traykovski et al., 2007; Wright et al., 2001, 1988)

$$Hg' \sin\alpha = C_D u_g |u_{max}| \quad (1)$$

where the left-hand and right-hand sides represent the buoyancy and friction terms, respectively. In equation (1), H is the thickness of the high-concentration layer (~10 cm), g' is the reduced gravity, $\sin\alpha$ is the seabed slope, C_D is the drag coefficient, u_g is the gravitational flow velocity, and u_{max} corresponds to the maximum velocity at the top of the high concentration layer, accounting for wave velocities and water column velocities, $u_{max} = \sqrt{u_w^2 + u_g^2 + u_c^2}$ (Wright et al., 2001). The downslope transport, which depends on the suspended sediment concentration and the gravitational velocity, can be estimated from equation (1) if the sediment concentration can be related to the wave forcing. This relationship is often expressed in terms of a bulk Richardson number (Trowbridge & Kineke, 1994; Wright & Friedrichs, 2006; Wright et al., 2001),

$$Ri_b = \frac{B}{u_{max}^2} \quad (2)$$

where $B = \frac{gs}{\rho_s}\int_0^H C(z)dz = g'H$ is the buoyancy anomaly integrated over the high-concentration layer of thickness H, $C(z)$ is the suspended sediment concentration (kg/m^3), s is the submerged weight of the sediment relative to seawater, and ρ_s is the density of the sediment. In general, both u_g and B are unknown and model closure can be achieved by assuming that the feedback between turbulence and suspended sediments maintains Ri_b at a critical value of $Ri_c = 0.25$ (Friedrichs & Wright, 2004; Scully et al., 2002, 2003; Trowbridge & Kineke, 1994); if $Ri_b > 0.25$ the damping of turbulence by stratification will cause sediment to settle, reducing Ri_b towards Ri_c, whereas if $Ri_b < 0.25$ the enhanced turbulence will resuspend more sediment causing Ri_b to increase back to Ri_c. Many recent models are based on equation (1) and use a critical $Ri_b = Ri_c$ for model closure (Friedrichs & Wright, 2004; Scully et al., 2002, 2003), assuming an unlimited supply of fine sediment that allows the turbid boundary layer to remain critically stratified at all times.

An alternative approach to modeling WSGF is to solve a mass balance within the high concentration near-bed layer, with gravitational velocities obtained from equation (1) and the entrainment of sediment into overlaying waters based on stratified mixing formulations (Chen et al., 2013; Harris et al., 2004, 2005; Traykovski et al., 2007). Sediment concentrations are related to the wave and current forcing in terms of bottom stresses and turbulence without invoking a critical Richardson number (Harris et al., 2004; Traykovski et al., 2007). While these models rely on parametrizations for a suite of near-bed processes such as settling speed, deposition, and erosion from the seabed, their applicability is not restricted to environments with an unlimited supply of fine sediment.

Although depositional patterns due to WSGFs have been successfully reproduced in several locations around the world using both types of models (Harris et al., 2004, 2005; Scully et al., 2002, 2003; Traykovski et al., 2007), neither the force balance, the critical Richardson number assumption, or the range of applicability of WSGF models have been rigorously tested in the field. Moreover, current observations suggest that WSGF are very limited in terms of locations and conditions. It is widely acknowledged, however, that the body of literature documenting these flows is still small and a complete understanding of the conditions required to generate them has not been achieved (Wright & Friedrichs, 2006), with the possibility that they are actually much more prevalent than expected.

In order to support downslope transport, sediment particles must generate a layer of very high concentration that influences the bulk density of the sediment-water suspension. It is generally assumed that this can only be achieved in fluid muds, in which hindered settling is significant, the particle size is small and the sediment concentration exceeds a threshold of approximately ~2–10 g/L (Winterwerp, 2002). Under these conditions the timescale for particle settling is long relative to timescales of the waves and turbulence. As a result of the above requirements for formation, the vast majority of observations of WSGF have been reported on continental shelves near the mouths of rivers where the combination of a large supply of fine sediment and high wave energy results in the resuspension of recently deposited and unconsolidated sediment (Hale & Ogston, 2015; Ma et al., 2010; Ogston et al., 2000; Traykovski et al., 2000, 2007). When samples of bottom sediments were acquired, field studies have predominantly reported distributions dominated by clays and silts, with mean (or median) particle sizes typically on the order of 4–8 μm and containing very small percentages of sand (Jaramillo et al., 2009; Ma et al., 2008; Traykovski et al., 2000, 2007).

2. Study Site and Methods

The Stratification Impacts on Nearshore Sediment (STRAINS) experiment made hydrodynamic and sediment transport measurements in the region of freshwater influence formed by the Rhine River along the Dutch coast in 2013 and 2014 (Flores et al., 2017; Horner-Devine et al., 2017). The measurements presented here document a WSGF event during the first major storm of the 2014 fall season (Figure 1c), which coincided with a period of low river outflow; discharge from the Rhine River was persistently below its annual average of 2,500 m^3/s during the 30 days prior to our deployment (Figure 1d). High waves and strong tides occur in this region and are mostly responsible for the observed sediment transport patterns (Flores et al., 2017; Pietrzak et al., 2011). Depth-averaged tidal currents are on the order of 1 m/s and severe storms during the fall and winter generate wind waves that can easily reach 4–5 m. Nonetheless, the conditions and setting are unique relative to previous observations of WSGF. The Rhine River is not a significant source of coastal sediments, with the exception of extreme flood events (Pietrzak et al., 2011), and seabed composition consists primarily of fine to medium sands with particle size ranging between 100 and 300 μm in 8–10 m depth and typically decreasing in the offshore direction (Janssen & Mulder, 2005).

The measurement location is adjacent to the Sand Engine (Stive et al., 2013), a mega nourishment project completed in 2012 (Figure 1a). While the emplacement of the Sand Engine undoubtedly provides a large source of coastal sediment, monitoring has shown that the particle size distribution around it has coarsened since its construction (Huisman et al., 2016). Moreover, observed suspended sediment concentrations are in the same range as those observed prior to its construction (Flores et al., 2017; Horner-Devine et al., 2017; van der Hout et al., 2015). This suggests that the Sand Engine does not provide a large source of fine sediments. Seafloor slopes and median grain sizes around the Sand Engine (Huisman et al., 2016) show values that are representative of many continental shelf areas; thus, while this is a unique setting in which a WSGF has been documented, it is not unique in terms of coastal morphology and sedimentology.

The measurement site was 10 km north of the Rhine River mouth and consisted of two frames, one in 8 m and one in 12 m of water (Figures 1a and 1b). Suspended sediment concentration and velocity profiles were obtained using acoustic and optical instrumentation. Down-looking acoustic backscattering systems (ABS) were used to estimate near-bottom sediment concentration profiles at both sites, with transducers measuring at frequencies of 1, 2, 3, and 4 MHz with 1-cm vertical resolution from approximately 1 m above the bottom to the seabed (Betteridge et al., 2008; Thorne et al., 2011). They were calibrated in the laboratory using particle size distributions representative of the field site. Sediment concentrations at four elevations (10, 20, 30, and 50 cmab) were collected using optical backscatter sensors (OBS) at the 8 m site, which were calibrated in the laboratory using sediment collected in the field. The ABS data are used primarily in the analyses since they provide much better vertical resolution, though the magnitude of the observed concentrations is confirmed in the OBS measurements.

Velocity profiles were measured using a combination of acoustic instruments. At the 8 m site, near-bed velocity profiles were obtained using a down-looking acoustic doppler profiler (Nortek Aquadopp) measuring at 2 Hz with 1-cm vertical resolution. An up-looking profiler measured velocities through the upper portion of the water column, with the first bin centered 1.6 m above the bottom and vertical resolution of 0.5 m. An ADV (acoustic Doppler velocimeter) was placed approximately 70 cm above the bottom and was used to connect the near-bottom and upper water column velocity profiles, as well as to obtain estimations of the bottom stress and drag coefficient. The velocity measurements were averaged in 10-min bursts and cubic splines were used to smooth vertical profiles. Unfortunately, the down-looking profiler at the 12 m site did not give usable data due to a battery malfunction. Data quality measures showed ping-to-ping correlations and signal-to-noise ratios within the recommended range of values in the near-bottom region. East-north velocity components were rotated to alongshore and cross-shore components using tidal ellipse properties, obtained by performing harmonic analysis (Pawlowicz et al., 2002) on the velocity data.

Bed elevation was determined using both the location of maximum acoustic backscatter (ABS) and the hydrodynamic bottom, where the mean velocities become zero in the down-looking Aquadopp data. In general, the surface of maximum acoustic backscatter agreed well with the location of zero mean velocities.

Wave orbital velocities were computed from the spectra of the ADV data over the typical wave frequency range from 0.02 to 0.3 Hz (Wiberg & Sherwood, 2008). Bed shear stress was calculated using a 1-D wave-current bottom boundary layer model (Grant & Madsen, 1986). Wave direction was estimated from directional data

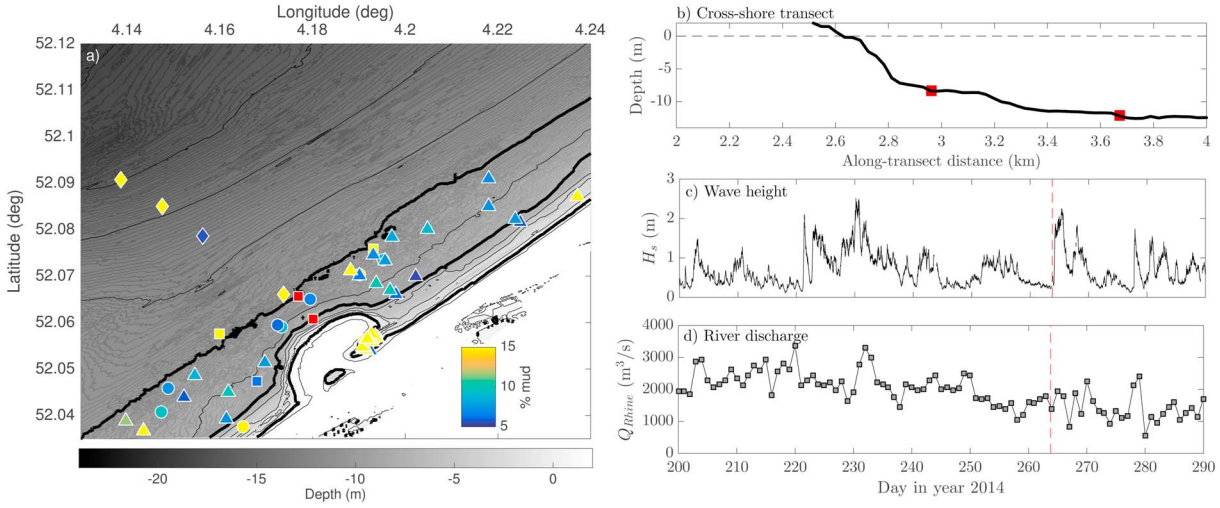

Figure 1. Study area, wave heights, and Rhine River discharge. (a) Bathymetry of the study area, including tripod locations (red squares). Thick black lines indicate the 0-, 8-, and 12-m-depth contours. Contours have been drawn every 2 m. Color squares, circles, and triangles represent locations with mud fraction greater than 5%, for surveys taken in October 2013, August 2014, and February 2015, respectively. Diamonds correspond to bed samples taken on deployment day, in September 2014 (b) Cross-shelf profile. Red squares mark tripod locations. (c) Significant wave height. (d) Rhine River discharge. Dashed red line in panels (c) and (d) indicate the beginning of the 2-day storm that generated the wave-supported gravity flow event.

from a WaveRider buoy located 1 km northeast of the measurement site, and bottom roughness was estimated from ripple heights (η) and wavelengths (λ) derived from an acoustic ripple profiler using $k_b = 27.7\eta^2/\lambda$ (Grant & Madsen, 1986).

3. Observations and Results

At the beginning of the storm, wave heights increased to 2.5 m (Figure 1c) resulting in near-bottom wave orbital velocities on the order of 0.45 m/s at the 12 m site (Figure 2a). Combined with the large tidal velocities in the area (De Boer et al., 2006; Rijnsburger et al., 2016), this resulted in high bed stresses that peaked during flood tides and showed an overall fivefold increase with respect to the preceding calm period (Figure 2a). Bottom stresses remained elevated for almost 2 days and reached values well above the threshold of resuspension for silts and fine sands. Following the large stresses, sediment concentration profiles measured by the ABSs showed maximum near-bottom concentrations of 40 (g/L) and 50 (g/L) at the 12 and 8 m sites (Figures 2b and 2c), respectively, which are of similar magnitude to those of previously reported WSGF events (Hale & Ogston, 2015; Traykovski et al., 2007). Peak concentrations of 10 (g/L) were reported by the OBS 20 cmab at the 8 m site (Figure 2b), suggesting that at times the high-concentration layer was at least 15–20 cm thick.

Significant bed elevation changes were observed during this event at both sites based on ABS data (Figures 2b and 2c). At the 12 m site, these changes resulted in approximately 10 cm of deposition over the course of the event with most of the deposition occurring within a few hours of the beginning of the storm, suggesting that the WSGF was initiated as soon as wave energy increased (Figure 2c). Records from pressure sensors on the frames did not show variations that could be related to instrument settling. The bed elevation also increased by more than 10 cm at the 8 m site; however, the net bed elevation change during the storm was only 5 cm (Figure 2b). The increase in concentration at the 12 m site lags that at the 8 m site by approximately 2 hr, which is consistent with downslope transport.

The velocity and sediment profiles during the event period reveal clear evidence of gravitational transport (Figure 3). Sediment concentration profiles at both sites show a high concentration layer with a thickness ranging between 5 and 20 cm and high concentration gradients (Figures 3g–3i). The concentration profiles show an exponential decay with maximum concentrations near the bed (Figures 3g–3i), similar to other field and laboratory experiments (Hooshmand et al., 2015; Lamb & Parsons, 2005; Souza et al., 2004; Traykovski et al., 2007).

Phase-averaged velocity profiles reveal the vertical structure of the current during slack, peak flood, and peak ebb tide periods (Figure 3). When tidal currents cease during slack, an offshore-directed jet is observed

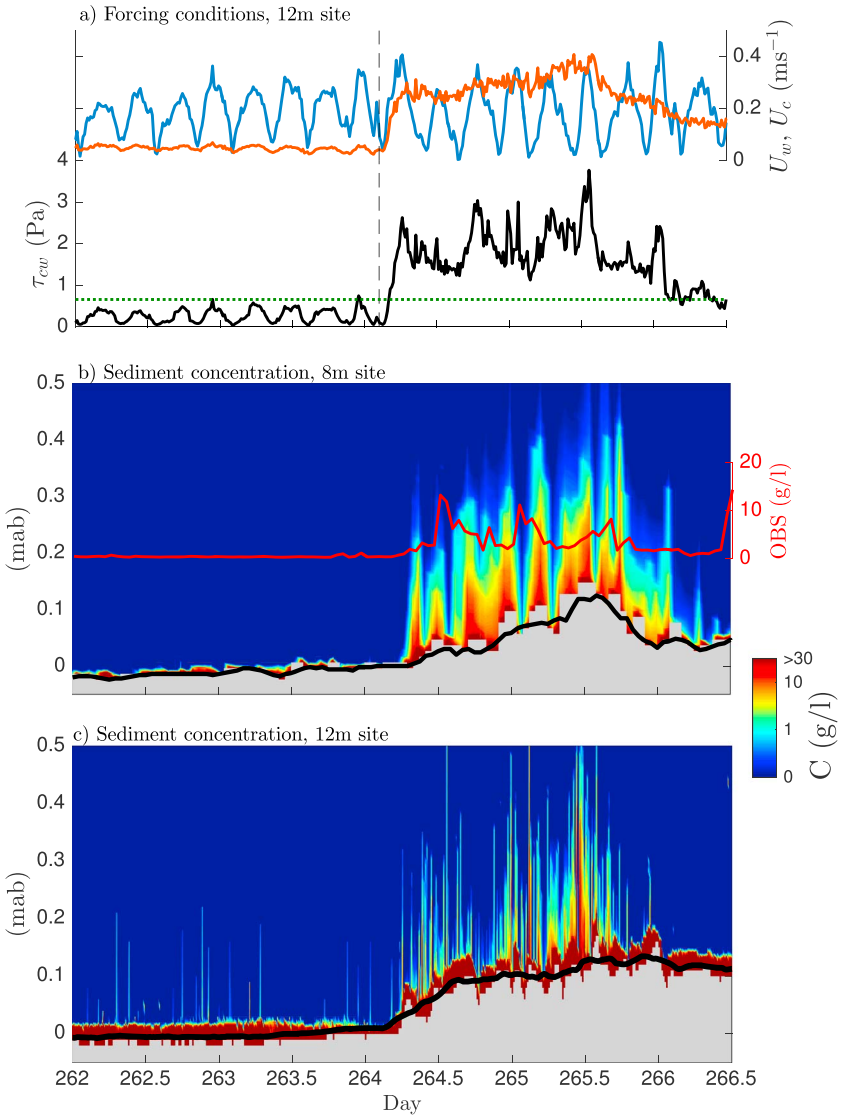

Figure 2. Forcing conditions and suspended sediment concentrations. (a) Near-bottom wave orbital velocity (red line), near-bottom tidal currents measured 0.25 mab (blue line) and combined wave-current bottom stress (black line) at the 12 m site. Vertical dashed line indicates the arrival of the storm. Horizontal dotted line indicates the critical stress for fine sand particles with d_{50} = 280 (μm) (b) Sediment concentrations at the 8 m site. Red line represents sediment concentrations measured by the optical backscatter sensors placed 20 cmab. (c) Sediment concentration at the 12 m site. The thick black lines in panels (b) and (c) correspond to a lowpass filter of the bed elevation.

in the lower 10 cm with weaker offshore flow above it (Figure 3d). The maximum average downslope flow during slack is approximately 2 cm/s; however, individual profiles show cross shore velocities reaching 5 cm/s (Figures 3e and 3d). This jet is attributed to gravitational flow since it occurs when other forcing ceases and it is vertically confined to the layer of high sediment concentration.

The tidal flow in this region is strongly influenced by density stratification associated with the nearby discharge from the Rhine River (Simpson & Souza, 1995; Visser et al., 1994), resulting in cross-shore tidal flow that is onshore during flood tide and offshore during ebb tide (Figures 3b–3c). Thus, the tidal current opposes the gravitational flow during flood tide, and we observe that this thins the layer of near-bed offshore flow, but does not completely suppress it (Figure 3e). In contrast, offshore tidal velocities during ebb tide thicken the near-bed layer to approximately 15 cm (Figure 3f). Tidal changes in the thickness of the high concentration layer are consistent with those observed in the velocity profiles; a thin layer during flood and thicker layers during slack and ebb. The alongshore velocity profiles are approximately logarithmic, although modification

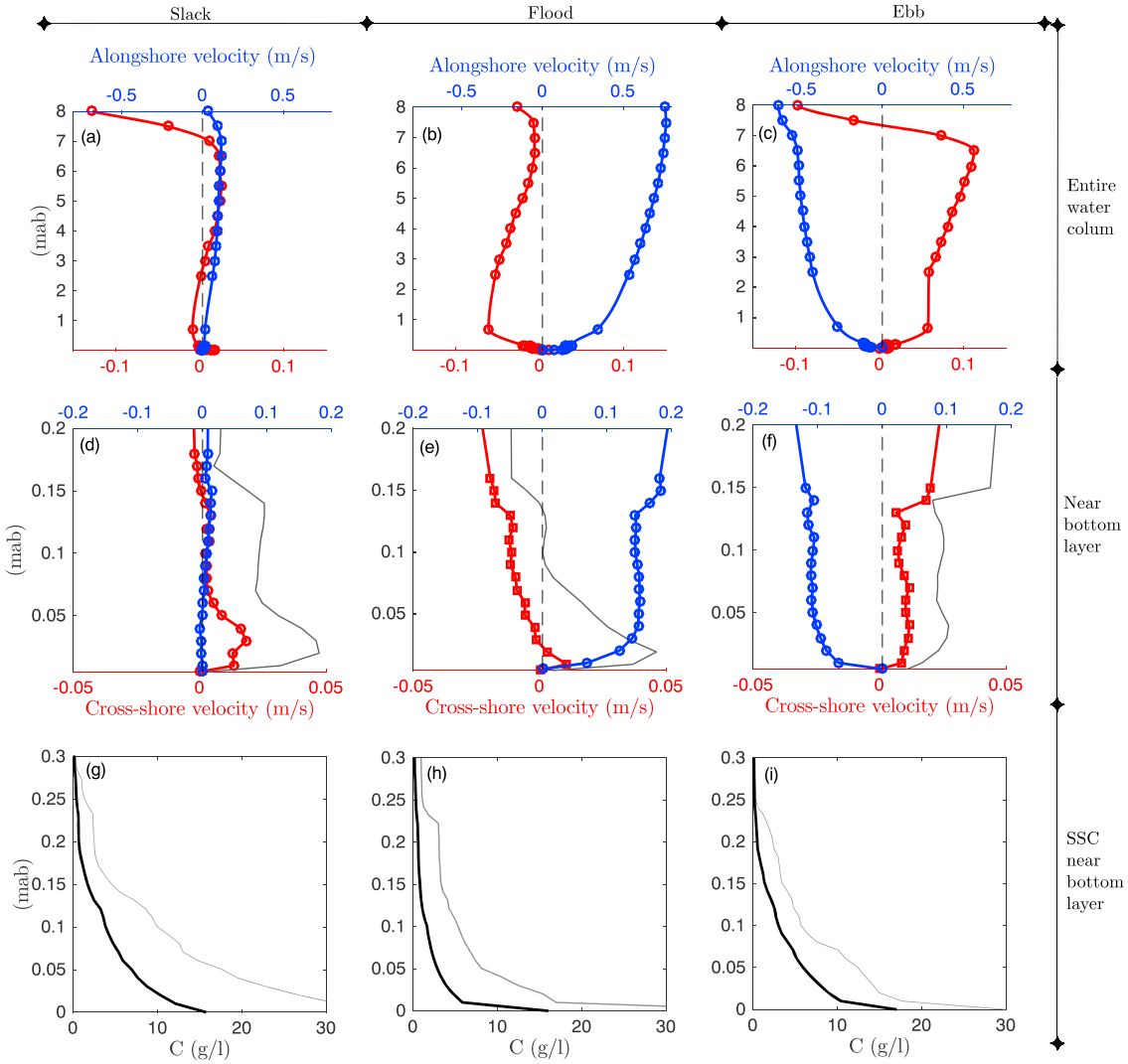

Figure 3. Velocity and sediment concentration profiles. (a–c) Alongshore (blue) and cross-shore (red) velocity profiles for the entire water column. (d–f) Alongshore (blue) and cross-shore (red) velocity profiles over the bottom 20 cm. Gray lines represent the envelope of maximum velocities. (g–i) Sediment concentration profiles over the bottom 30 cm. Gray lines correspond to the envelope of maximum observed concentrations at each elevation. Velocity and concentration profiles correspond to phase averages for the slack, peak flood, and peak ebb tidal phases. Each profile was computed using between 6 and 8 individual profiles. Individual profiles were obtained by averaging the 2-Hz data into 10-min bursts. Positive values correspond to flow directed to the northeast (alongshore) and offshore (cross shore).

in the profile due to the influence of stratification is expected (Figures 3a–3c). Despite these modulations of the layer thickness by tidal velocities, the average layer thickness remains small (0.05–0.20 m) compared with the much thicker turbid layers (1–2 m) observed in systems in which stress from currents are of first-order importance to the dynamics of the gravity flow (Ma et al., 2010, 2008). Thus, the dynamics of the gravity flow observed here appear to be dominated by wave stress, even though tidal currents also exert an influence on their structure and direction.

The high concentrations observed during the WSGF resulted in elevated cross-shore sediment transport (Figure 4d). The net cross-shore sediment flux due to the WSGF event was an order of magnitude greater than the suspended load transport in the overlying water column (0.5 mab to the surface) measured nearby at the 12 m site (Flores et al., 2017) or the bedload transport based on the formula of Madsen (1991) for the same time period (Figure 4d). In fact, the offshore transport during this 1.5-day WSGF event was much higher than the suspended sediment transport observed during a 30-day period at the nearby 12 m site. Sediment concentration measurements were not made in the upper water column at the 8 m site.

4. Gravitational Velocity, Force Balance, and Richardson Number

The gravitational velocity component, u_g, can be estimated using our near-bed measurements and the force balance presented in equation (1). The thickness of the high concentration layer, H, and the reduced gravity, g', are estimated directly from the sediment concentration profiles (Traykovski et al., 2007). The seabed slope at the 8 m site was estimated from bathymetry data as $\alpha = 0.008$. The maximum velocity u_{max} was computed including wave, current and gravitational velocities. The value for the drag coefficient at the 8 m site was estimated as $C_D = 0.003$, based on the ADV turbulence measurements outside the wave boundary layer. This value is consistent with values used in previous WSGF studies (Scully et al., 2002, 2003). A detailed presentation of the methods for estimating C_D and its tidal variability are presented in the supplemental information. Figure 4c shows the comparison between u_g predicted from equation (1) and the measured cross-shore velocity averaged over the high-concentration layer, U_{cross}. Although predicted u_g values are almost always greater than the observed cross-shore velocity, the variability in U_{cross} is well explained by the u_g prediction during slack tides ($R^2 = 0.92$, Figure 4c—inset), which suggests that U_{cross} responds directly to changes in the sediment-induced buoyancy, B (equation (1)). However, the tidally influenced variability in U_{cross} exceeds that due to changes in buoyancy except close to slack tide (Figure 4c). This is particularly true during flood tides, when the poorest agreement between U_{cross} and u_g is observed as the onshore tidal flow opposes the gravitational flow (Figure 4c and Figure 3).

In order to evaluate the subtidal momentum balance (equation (1)) we set $u_g = 1.6$ cm/s, which corresponds to the average magnitude of U_{cross} during slack tides. This provides a representative gravitational velocity that results from the available sediment-induced buoyancy, without significant tidal influence. Using the mean observed slack tide cross-shore velocity for u_g, the frictional and gravitational terms balance to within 6% after an initial adjustment period (Figure 5b). This good agreement supports previous findings suggesting that WSGF dynamics are governed by a buoyancy-friction balance (Traykovski et al., 2007) and further confirms that the observed flow is indeed a WSGF. The initial adjustment provides information on the initiation and temporal evolution of WSGF. Immediately after the start of the storm the wave forcing, via the friction term, exceeds the buoyancy term, suggesting that the high concentration layer may still be forming. Subsequently, the buoyancy term exceeds the friction term for several hours. This imbalance may have been caused by a slumping event that occurred shortly after the wave energy increased, which may also help to explain the sudden change in bed elevation observed at the 12 m site (Figure 2c). The high near-bottom offshore velocities also support the hypothesis that strong gravitational flow occurred during the initial stage of the storm (Figure 4c).

The bulk Richardson number is relatively constant, with the exception of a few hours early in the storm (Figure 5c). The constant value observed after day 264.8 supports the hypothesis that a dynamical feedback is established, forming a quasi-steady suspension (Wright et al., 2001). However, we observe a constant value of $Ri_b = 0.01$, which is more than one order of magnitude lower than the canonical value of $Ri_b = 0.25$ typically assumed in WSGF models (Friedrichs & Scully, 2007; Friedrichs & Wright, 2004; Scully et al., 2002; Wright et al., 2001).

5. Discussion

5.1. Modeling WSGF

The Richardson number is one of the key parameters often used in the modeling of WSGF. Although $Ri_b = 0.25$ has been widely adopted, data from several previous studies also result in values of the Richardson number below this critical value (Hsu et al., 2009; Lamb & Parsons, 2005; Traykovski et al., 2007). Low values of Ri_b, such as those observed in this study, have been ascribed to finite bed erodibility (Hsu et al., 2009). On the Dutch coast it is likely that low erodibility results from the high sand content in the bed; winnowing of fine sediment from the bed during the initial stages of the event will coarsen the bed and reduce erodibility.

In order to test the applicability of WSGF models to our observations, we have estimated gravitational velocities using constant Richardson numbers ($Ri_b = 0.25$ and $Ri_b = 0.01$) and a 1-D WSGF mass balance model (Traykovski et al., 2007). These estimates are shown in Figure 5d. For the vertical mass balance model, we have included estimates using both low and high erodibility coefficients (commonly referred to as γ_0). As these models rely on the use of Equation 1 but differ on how they estimate sediment concentrations, the gravitational velocities in Figure 5d have been normalized by $u_g(C_{meas})$. This represents the gravitational velocities obtained from Equation 1 using the measured sediment concentrations profiles (as in Figure 4c),

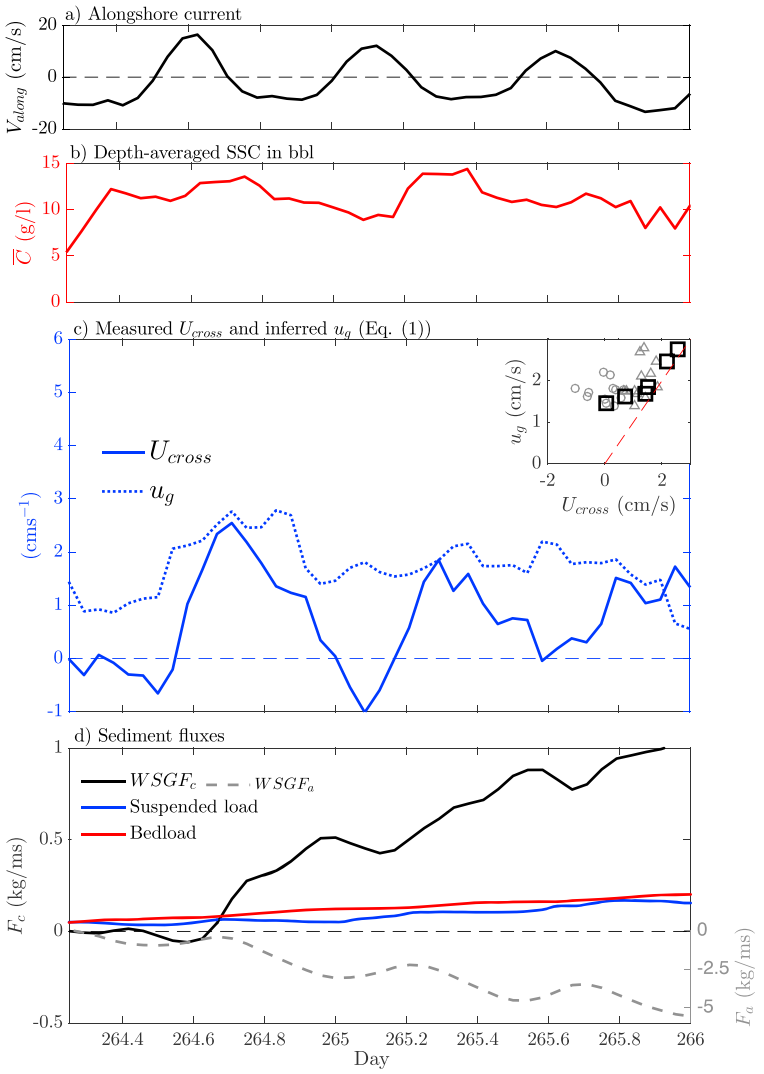

Figure 4. Velocity components and sediment fluxes. (a) Near-bed alongshore current (positive for flood tide, negative for ebb tide). (b) Depth-averaged suspended sediment concentration in the turbid near-bottom boundary layer. (c) Gravitational velocity (u_g, dotted blue line), as inferred from the force balance (equation (1)), vertically averaged cross-shore velocity over the high-concentration layer (U_{cross}, solid blue line). Inset shows a scatter plot comparison between u_g and U_{cross} for slack (black squares), ebb (gray triangles) and flood (gray circles) tidal phases. (d) Cumulative cross-shore sediment fluxes for the WSGF event (black line), measured suspended load at the nearby 12 m site (blue line) and estimated bedload (red line), and cumulative alongshore flux for the WSGF event (gray dotted line, axis on the right). Positive cross-shore fluxes are offshore, positive alongshore fluxes are directed northwards. WSGF = wave-supported gravity flow.

which we consider to be the best estimation these models could provide. For reference, we have also included the measured cross-shore velocities, U_{cross}. The best agreement is achieved with the use of $Ri_b = 0.01$, although $u_g(Ri = 0.01)$ underpredicts $u_g(C_{meas})$ at times when the peak in Ri_b is observed (Figure 5c, around day 264.6). The use of $Ri_b = 0.25$ results in u_g values with a mean of 27 cm/s, an order of magnitude higher than the observed velocities or $u_g(C_{meas})$. The mass balance model gives results that are much closer to $u_g(C_{meas})$, with estimates obtained using low bed erodibility showing a better performance overall than those obtained with high erodibility.

The models used in our comparison differ in terms of the physical processes that are assumed to be responsible for limiting cross-shore transport in WSGF. The use of $Ri_b = 0.25$ assumes that sediment availability is unlimited and that the high suspension layer is critically stratified. This model significantly overpredicts transport in the observed WSGC. However, Ri_b is observed to be constant during most of the WSGF event,

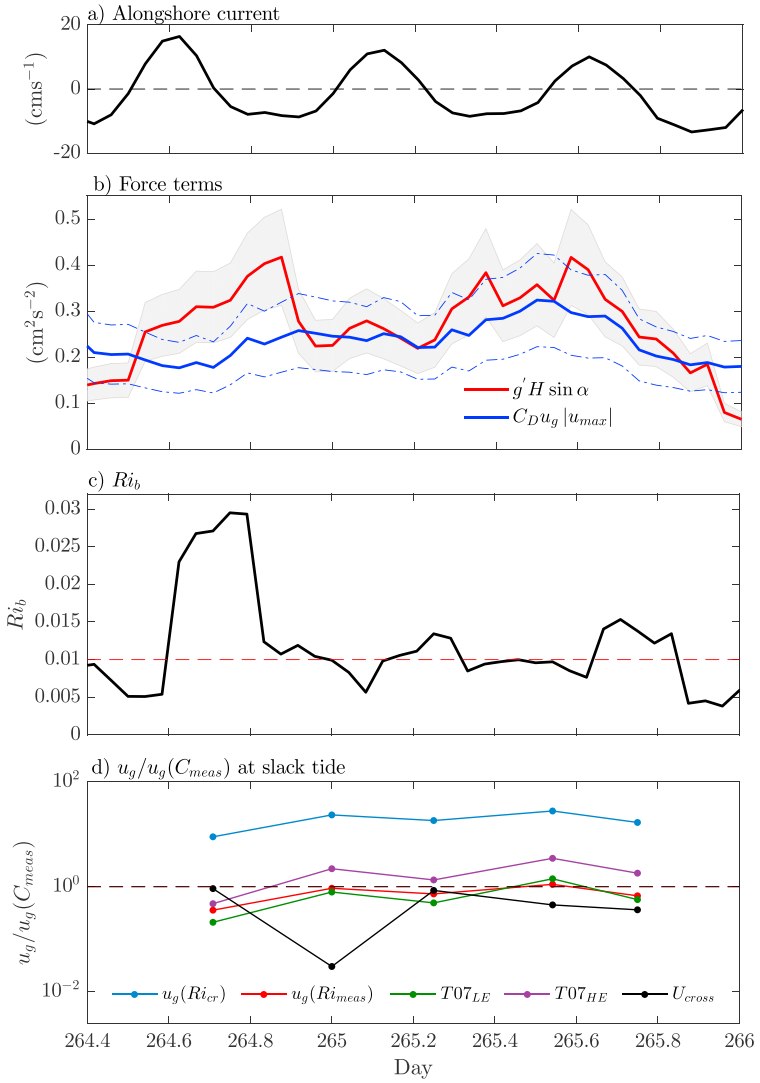

Figure 5. Dynamics of the Wave-supported gravity flow. (a) Alongshore current (positive is flood tide, negative is ebb tide). (b) Chezy balance: gravitational (solid red line) and frictional (solid blue line) terms. Gray area is associated to the uncertainty in seabed slope (±20%). Dashed blue line is associated to the uncertainty in u_g, determined based on the standard deviation of u_g during slack tides. (c) Richardson number (equation (2)). (d) Gravitational velocities at slack tide, normalized by $u_g(C_{meas})$ (see text for definition). Gravitational velocity inferred from equation (1) using a critical Richardson number ($R_c = 0.25$, blue), gravitational velocity inferred from equation (1) using measured Richardson number ($Ri = 0.01$, red), gravitational velocity obtained from Traykovski et al. (2007) 1-D model using a resuspension parameter $\gamma_0 = 0.002$ ($T07_{LE}$, green), gravitational velocity obtained from Traykovski et al. (2007) 1-D model using a resuspension parameter $\gamma_0 = 0.005$ ($T07_{HE}$, purple), and measured cross-shore velocity (U_{cross}, black).

albeit at a value much lower than 0.25, suggesting that a critical Ri_b model may still be appropriate. Use of such a model for coarse particle suspensions would require a suitable prediction of Ri_b. In the mass balance model (Traykovski et al., 2007), on the other hand, sediment suspension is limited by erosion from the seabed. This model compares well with the current observations, especially when the bed erodibility is assumed to be low.

5.2. The Role of Fine Sediment

Hindered settling, which occurs preferentially in fine sediments, is thought to be a key component in the maintenance of high-density suspensions (Winterwerp, 2002). This suggests that fine sediment is likely to have played an important role in the observed WSGF, despite the fact that the bed sediment is predominantly sandy. Our measurements did not resolve the particle size distribution of the sediment suspension, and thus we cannot determine the fraction of fine sediment present in the high concentration layer or how important fine sediment was in the generation of the WSGF.

Field surveys have confirmed the presence of fines in the region; mud deposits and areas with high turbidity are frequently observed off the Dutch coast and along the southern bight of the North Sea (Fettweis & Van den Eynde, 2003; Van Alphen, 1990; van der Hout et al., 2015, 2017; Visser et al., 1991). Detailed surveys of the size distribution of sands (Huisman et al., 2016) give a reasonable estimate of the fraction of fine sediment (<63μm) on the seabed and the spatial and temporal variability of transient mud deposits close to our measurement sites (Figure 1a). Locations with seabed fine sediment fractions greater than 5% were frequently observed all around the measurement sites, and some of them showed fractions reaching up to 30% particularly near the 12-m isobath (Figure 1a). Hindered settling has been shown to occur when the sediment concentration exceeds 2–10 g/L (Winterwerp, 2002). Near-bed concentrations of fine sediment in this range can be achieved even in this relatively coarse mixture considering that the observed near-bed concentrations ranged from 10–50 g/L (Figures 3 and 4b) and bed fractions ranged from 5% to 30%. This estimate assumes that the high concentration layer has a similar size distribution to the seabed. While this is not know, winnowing may actually result in a finer size distribution in the layer than on the seabed.

6. Summary

The movement of sediment across gently sloping continental shelves has long been one of the most poorly understood components of source-to-sink sediment budgets (Nittrouer & Wright, 1994). Previous studies have identified WSGF as a leading process for cross-shelf transport of muds, but the measurements presented here are the first to document the importance of WSGF to cross-shelf transport and morphological evolution on sandy inner shelves. Offshore transport associated with this 1.5-day WSGF event was much higher than estimates of bedload transport and measurements of suspended sediment transport at a nearby site during a 30-day period. During this period WSGF was the dominant mechanism of cross-shore transport in this region, however, the frequency of occurrence is unknown.

The observed WSGF dynamics support the use of the Chezy balance for modeling WSGF on sandy seabeds. They also suggest that particle size plays a key role in determining the intensity of downslope transport and that a critical Richardson number ($Ri_c = 0.25$) cannot be achieved in sandy environments. Coarse particles may influence WSGF transport either by modifying the dynamics of the turbulent suspension due to higher settling rates or by reducing the bed erodibility. Future work is necessary to determine the relative importance of these processes in limiting transport in mixed sediment suspensions.

Nonetheless, the occurrence of this event under conditions unique from previous observations suggests that WSGF may occur more frequently and in a much wider range of shelf locations than previously thought.

Acknowledgments
The authors would like to thank Bas Huisman, Jeroen Wijsman, and Pieter-Koen Tonnon for providing seabed sample data; Richard Cooke, Christopher Balfour, and the crew of the R/V Zirfaea for their technical support during the measurements; Rijkswaterstaat for their generous and kind support; and NERC for support provided to deploy the MiniStable frame. The authors are grateful from support from the Netherlands Organization for Scientific Research STW program Project12682 and ERC-advanced grant 291206Nearshore Monitoring and Modeling (NEMO). R. P. F. would like to thank the Fulbright Commission and CONICYT-Chile for the scholarship provided. A. R. H.-D. is grateful for support from NSF grant OCE-1537435. Data from the paper are available at https://doi.org/10.4121/uuid:e1fe526d-cf17-4332-983c-97c3a56b0ddf. Remaining data from the project will be archived in National Data Centers in the UK and The Netherlands upon completion of the research project.

References

Betteridge, K. F., Thorne, P. D., & Cooke, R. D. (2008). Calibrating multi-frequency acoustic backscatter systems for studying near-bed suspended sediment transport processes. *Continental Shelf Research*, *28*, 227–235. https://doi.org/10.1016/j.csr.2007.07.007

Chen, S.-N., Geyer, W. R., & Hsu, T.-J. (2013). A numerical investigation of the dynamics and structure of hyperpycnal river plumes on sloping continental shelves. *Journal of Geophysical Research: Oceans*, *118*, 2702–2718. https://doi.org/10.1002/jgrc.20209

De Boer, G. J., Pietrzak, J. D., & Winterwerp, J. C. (2006). On the vertical structure of the rhine region of freshwater influence. *Ocean dynamics*, *56*, 198–216. https://doi.org/10.1007/s10236-005-0042-1

Fettweis, M., & Van den Eynde, D. (2003). The mud deposits and the high turbidity in the belgian–dutch coastal zone, southern bight of the north sea. *Continental Shelf Research*, *23*(7), 669–691. https://doi.org/10.1016/S0278-4343(03)00027-X

Flores, R. P, Rijnsburger, S, Horner-Devine, A. R., Souza, A. J., & Pietrzak, J. D. (2017). The impact of storms and stratification on sediment transport in the rhine region of freshwater influence. https://doi.org/10.1002/2016JC012362

Friedrichs, C. T., & Scully, M. E. (2007). Modeling deposition by wave-supported gravity flows on the po river prodelta: From seasonal floods to prograding clinoforms. *Continental Shelf Research*, *27*, 322–337. https://doi.org/10.1016/j.csr.2006.11.002

Friedrichs, C., & Wright, L. (2004). Gravity-driven sediment transport on the continental shelf: Implications for equilibrium profiles near river mouths. *Coastal Engineering*, *51*, 795–811. https://doi.org/10.1016/j.coastaleng.2004.07.010

Grant, W. D., & Madsen, O. S. (1986). The continental-shelf bottom boundary layer. *Annual Review of Fluid Mechanics*, *18*(1), 265–305.

Hale, R. P., & Ogston, A. S. (2015). In situ observations of wave-supported fluid-mud generation and deposition on an active continental margin. *Journal of Geophysical Research: Earth Surface*, *120*, 2357–2373. https://doi.org/10.1002/2015JF003630

Harris, C. K., Traykovski, P., & Geyer, W. R. (2004). *Including a near-bed turbid layer in a three dimensional sediment transport model with application to the Eel River shelf* (pp. 784–803). Northern California: Estuarine and Coastal Modeling 2003.

Harris, C. K., Traykovski, P. A., & Geyer, W. R. (2005). Flood dispersal and deposition by near-bed gravitational sediment flows and oceanographic transport: A numerical modeling study of the eel river shelf, northern California. *Journal of Geophysical Research: Oceans*, *110*, C09025. https://doi.org/10.1029/2004JC002727

Hooshmand, A., Horner-Devine, A. R., & Lamb, M. P. (2015). Structure of turbulence and sediment stratification in wave-supported mud layers. *Journal of Geophysical Research: Oceans*, *120*, 2430–2448. https://doi.org/10.1002/2014JC010231

Horner-Devine, A. R., Pietrzak, J. D., Souza, A. J., McKeon, M. A., Meirelles, S., Henriquez, M., et al. (2017). Cross-shore transport of nearshore sediment by river plume frontal pumping. *Geophysical Research Letters*, *44*, 6343–6351.

Hsu, T. J., Ozdemir, C. E., & Traykovski, P. A. (2009). High-resolution numerical modeling of wave-supported gravity-driven mudflows. *Journal of Geophysical Research*, *114*, C05014. https://doi.org/10.1029/2008JC005006

Huisman, B., De Schipper, M., & Ruessink, B. (2016). Sediment sorting at the sand motor at storm and annual time scales. *Marine Geology*, *381*, 209–226. https://doi.org/10.1016/j.margeo.2016.09.005

Janssen, G., & Mulder, S. (2005). Zonation of macrofauna across sandy beaches and surf zones along the dutch coast. *Oceanologia*, *47*, 265–282.

Jaramillo, S., Sheremet, A., Allison, M., Reed, A., & Holland, K. (2009). Wave-mud interactions over the muddy atchafalaya subaqueous clinoform, louisiana, United States: Wave-supported sediment transport. *Journal of Geophysical Research*, *114*, C04002. https://doi.org/10.1029/2008JC004821

Lamb, M. P., & Parsons, J. D. (2005). High-density suspensions formed under waves. *Journal of Sedimentary Research*, *75*, 386–397. https://doi.org/10.2110/jsr.2005.030

Ma, Y., Friedrichs, C. T., Harris, C. K., & Wright, L. D. (2010). Deposition by seasonal wave-and current-supported sediment gravity flows interacting with spatially varying bathymetry: Waiapu shelf, New Zealand. *Marine Geology*, *275*, 199–211.

Ma, Y., Wright, L. D., & Friedrichs, C. T. (2008). Observations of sediment transport on the continental shelf off the mouth of the Waiapu river, New Zealand: Evidence for current-supported gravity flows. *Continental Shelf Research*, *28*, 516–532. https://doi.org/10.1016/j.csr.2007.11.001

Macquaker, J. H., Bentley, S. J., & Bohacs, K. M. (2010). Wave-enhanced sediment-gravity flows and mud dispersal across continental shelves: Reappraising sediment transport processes operating in ancient mudstone successions. *Geology*, *38*, 947–950.

Madsen, O. S. (1991). Mechanics of cohesionless sediment transport in coastal waters, coastal sediments.

Nittrouer, C. A., & Wright, L. D. (1994). Transport of particles across continental shelves. *Reviews of Geophysics*, *32*(1), 85–113.

Ogston, A., Cacchione, D., Sternberg, R., & Kineke, G. (2000). Observations of storm and river flood-driven sediment transport on the northern california continental shelf. *Continental Shelf Research*, *20*(16), 2141–2162.

Parsons, J. D, Friedrichs, C. T, Traykovski, P. A, Mohrig, D, Imran, J, Syvitski, J. P, et al. (2007). The mechanics of marine sediment gravity flows. In C. Nittrouer, J. Austin, M. Field, J. Syvitski, & P. Wiberg (Eds.), *Continental margin sedimentation: From sediment transport to sequence stratigraphy* (pp. 275–333). UK.

Pawlowicz, R., Beardsley, B., & Lentz, S. (2002). Classical tidal harmonic analysis including error estimates in matlab using t_tide. *Computers and Geosciences*, *28*(8), 929–937.

Pietrzak, J. D., de Boer, G. J., & Eleveld, M. A. (2011). Mechanisms controlling the intra-annual mesoscale variability of SST and SPM in the southern north sea. *Continental Shelf Research*, *31*, 594–610. https://doi.org/10.1016/j.csr.2010.12.014

Puig, P., Ogston, A., Mullenbach, B., Nittrouer, C., Parsons, J., & Sternberg, R. (2004). Storm-induced sediment gravity flows at the head of the eel submarine canyon, northern california margin. *Journal of Geophysical Research*, *109*, C03019. https://doi.org/10.1029/2003JC001918

Puig, P., Ogston, A., Mullenbach, B., Nittrouer, C., & Sternberg, R. (2003). Shelf-to-canyon sediment-transport processes on the eel continental margin northern california. *Marine Geology*, *193*(1), 129–149. https://doi.org/10.1016/S0025-3227(02)00641-2

Rijnsburger, S., van der Hout, C. M., van Tongeren, O., de Boer, G. J., van Prooijen, B. C., Borst, W. G., & Pietrzak, J. D. (2016). Simultaneous measurements of tidal straining and advection at two parallel transects far downstream in the rhine ROFI. *Ocean Dynamics*, *66*, 719–736. https://doi.org/10.1007/s10236-016-0947-x

Scully, M., Friedrichs, C., & Wright, L. (2002). Application of an analytical model of critically stratified gravity-driven sediment transport and deposition to observations from the eel river continental shelf, Northern California. *Continental Shelf Research*, *22*(14), 1951–1974.

Scully, M., Friedrichs, C., & Wright, L. (2003). Numerical modeling of gravity-driven sediment transport and deposition on an energetic continental shelf: Eel river, northern california. *Journal of Geophysical Research*, *108*(C4), 3120. https://doi.org/10.1029/2002JC001467

Simpson, J., & Souza, A. (1995). Semidiurnal switching of stratification in the region of freshwater influence of the rhine. *Journal of Geophysical Research*, *100*(C4), 7037–7044.

Souza, A. J., Alvarez, L. G., & Dickey, T. D. (2004). Tidally induced turbulence and suspended sediment. *Geophysical Research Letters*, *31*, L20309. https://doi.org/10.1029/2004GL021186

Stive, M. J., de Schipper, M. A., Luijendijk, A. P., Aarninkhof, S. G., van Gelder-Maas, C., van Thiel de Vries, J. S., et al. (2013). A new alternative to saving our beaches from sea-level rise: The sand engine. *Journal of Coastal Research*, *29*, 1001–1008. https://doi.org/10.2112/JCOASTRES-D-13-00070.1

Thorne, P. D., Hurther, D., & Moate, B. D. (2011). Acoustic inversions for measuring boundary layer suspended sediment processes. *Journal of the Acoustical Society of America*, *130*, 1188–1200. https://doi.org/10.1121/1.3618728.

Traykovski, P., Geyer, W. R., Irish, J., & Lynch, J. (2000). The role of wave-induced density-driven fluid mud flows for cross-shelf transport on the eel river continental shelf. *Continental Shelf Research*, *20*(16), 2113–2140.

Traykovski, P., Wiberg, P. L., & Geyer, W. R. (2007). Observations and modeling of wave-supported sediment gravity flows on the po prodelta and comparison to prior observations from the eel shelf. *Continental Shelf Research*, *27*, 375–399. https://doi.org/10.1016/j.csr.2005.07.008

Trowbridge, J., & Kineke, G. (1994). Structure and dynamics of fluid muds on the Amazon continental shelf. *Journal of Geophysical Research*, *99*(C1), 865–874.

Van Alphen, J. (1990). A mud balance for Belgian-Dutch coastal waters between 1969 and 1986. *Netherlands Journal of Sea Research*, *25*(1-2), 19–30.

van der Hout, C. M., Gerkema, T., Nauw, J. J., & Ridderinkhof, H. (2015). Observations of a narrow zone of high suspended particulate matter (SPM) concentrations along the dutch coast. *Continental Shelf Research*, *95*, 27–38. https://doi.org/10.1016/j.csr.2015.01.002

van der Hout, C., Witbaard, R., Bergman, M., Duineveld, G., Rozemeijer, M., & Gerkema, T. (2017). *The dynamics of suspended particulate matter (SPM) and chlorophyll-a from intratidal to annual time scales in a coastal turbidity maximum* (Vol. 127, pp. 105–118). https://doi.org/10.1016/j.seares.2017.04.011

Visser, M., De Ruijter, W., & Postma, L. (1991). The distribution of suspended matter in the dutch coastal zone. *Netherlands Journal of Sea Research*, *27*(2), 127–143.

Visser, A., Souza, A., Hessner, K., & Simpson, J. (1994). The effect of stratification on tidal current profiles in a region of fresh-water influence. *Oceanologica acta*, *17*(4), 369–381.

Walsh, J., Nittrouer, C., Palinkas, C., Ogston, A., Sternberg, R., & Brunskill, G. (2004). Clinoform mechanics in the Gulf of Papua New Guinea. *Continental Shelf Research*, *24*, 2487–2510. https://doi.org/10.1016/j.csr.2004.07.019

Wiberg, P. L., & Sherwood, C. R. (2008). Calculating wave-generated bottom orbital velocities from surface-wave parameters. *Computers and Geosciences*, *34*, 1243–1262. https://doi.org/10.1016/j.cageo.2008.02.010

Winterwerp, J. (2002). On the flocculation and settling velocity of estuarine mud. *Continental Shelf Research*, *22*(9), 1339–1360.

Wright, L., & Friedrichs, C. (2006). Gravity-driven sediment transport on continental shelves: A status report. *Continental Shelf Research*, *26*, 2092–2107. https://doi.org/10.1016/j.csr.2006.07.008

Wright, L., Friedrichs, C., Kim, S., & Scully, M. (2001). Effects of ambient currents and waves on gravity-driven sediment transport on continental shelves. *Marine Geology*, *175*(1), 25–45.

Wright, L., Wiseman, W., Bornhold, B., Prior, D., Suhayda, J., Keller, G., et al. (1988). Marine dispersal and deposition of yellow river silts by gravity-driven underflows. *Nature*, *332*, 629–632.